

Deformable Groupwise Registration Using a Locally Low-Rank Dissimilarity Metric for Myocardial Strain Estimation from Cardiac Cine MRI Images

Haiyang Chen, Juan Gao, and Chenxi Hu*, *Member, IEEE*

Abstract— Objective: Cardiovascular magnetic resonance-feature tracking (CMR-FT) represents a group of methods for myocardial strain estimation from cardiac cine MRI images. Established CMR-FT methods are mainly based on optical flow or pairwise registration. However, these methods suffer from either inaccurate estimation of large motion or drift effect caused by accumulative tracking errors. In this work, we propose a deformable groupwise registration method using a locally low-rank (LLR) dissimilarity metric for CMR-FT. **Methods:** The proposed method (Groupwise-LLR) tracks the feature points by a groupwise registration-based two-step strategy. Unlike the globally low-rank (GLR) dissimilarity metric, the proposed LLR metric imposes low-rankness on local image patches rather than the whole image. We quantitatively compared Groupwise-LLR with the Farneback optical flow, a pairwise registration method, and a GLR-based groupwise registration method on simulated and in vivo datasets. **Results:** Results from the simulated dataset showed that Groupwise-LLR achieved more accurate tracking and strain estimation compared with the other methods. Results from the in vivo dataset showed that Groupwise-LLR achieved more accurate tracking and elimination of the drift effect in late-diastole. Inter-observer reproducibility of strain estimates was similar between all studied methods. **Conclusion:** The proposed method estimates myocardial strains more accurately due to the application of a groupwise registration-based tracking strategy and an LLR-based dissimilarity metric. **Significance:** The proposed CMR-FT method may facilitate more accurate estimation of myocardial strains, especially in diastole, for clinical assessments of cardiac dysfunction.

Index Terms—feature tracking, groupwise registration, locally low-rank, motion estimation, myocardial strain

I. INTRODUCTION

MYOCARDIAL strain is a sensitive measure of left ventricular (LV) mechanical function, both globally and regionally. Previous studies have shown its potential to identify sub-clinical LV dysfunction in cardiomyopathies[1]. Cardiovascular magnetic resonance-feature tracking (CMR-FT)

represents a group of methods that estimate myocardial strains from routinely performed balanced steady-state free-precession (bSSFP) cine images[2]. Compared with the reference standard tagging-MRI, CMR-FT does not need additional time-consuming sequences and enables retrospective analysis for patients who did not undergo strain imaging[3], [4]. These advantages render CMR-FT appealing in a clinical setting.

Current mainstream CMR-FT methods are mainly based on optical flow or pairwise registration[5]–[7]. These methods employ pairwise alignment of images, by either aligning every image to the end-diastolic (ED) image or sequentially aligning each pair of neighboring images. However, the first approach could be inaccurate for image pairs with a large cardiac motion (e.g., between ED and end-systole (ES))[8], [9], while the second approach suffers from a drift effect caused by the accumulation of tracking errors over the cardiac cycle[5], [10]. A post hoc method to compensate for the drift effect is to approximate the drift by a linear function and subtract it from the estimated strain curve[11], [12]. However, since the linearity of the drift is assumed only for simplicity, the compensation is highly empirical and does not truly eliminate the accumulative tracking errors. On the contrary, groupwise registration has the potential to eliminate the drift effect by simultaneously aligning all cine images to a common reference frame. A variety of metrics for groupwise registration have been explored, including but not limited to extended normalized mutual information[13], voxelwise signal entropies[14], low-dimensionality of signal models[15], and low-rankness between aligned images[16], [17]. However, although an improved tracking of the myocardium has been reported for some groupwise registration methods[18], [19], their accuracy and reproducibility in terms of strain estimates have not been fully explored. Whether the more accurate tracking can translate to a more accurate or reproducible strain estimation awaits to be answered.

Furthermore, it is well-known that dynamic signals in MRI images are often locally low-ranked rather than globally low-

This work was supported in part by National Natural Science Foundation of China (No. 62001288) and Shanghai Science and Technology Commission (No. 22TS1400200).

H. Chen is with School of Biomedical Engineering, Shanghai Jiao Tong University, Shanghai, China. J. Gao is with School of Biomedical Engineering,

Shanghai Jiao Tong University, Shanghai, China. C. Hu is with School of Biomedical Engineering, Shanghai Jiao Tong University, Shanghai, China (correspondence e-mail: chenxi.hu@sjtu.edu.cn).

ranked[20], [21]. Different tissues encompass signal variations of different patterns, and thus the global rank can be relatively high even after performing motion correction. For example, the blood pool often contains transient flow artifacts, and the myocardium often experiences periodic signal increases and decreases due to through-plane myocardial motion. These signal variations are unique to the corresponding tissue and the inclusion of all of them for rank evaluation would cause an increase of rank. Therefore, a Locally Low-Rank (LLR) criterion may be a better metric to measure the alignment of cine images over the cardiac cycle. However, existing low-rank-based dissimilarity metrics for groupwise registration only exploit the Global Low-Rank (GLR) property between aligned images[17], [22]. In this work, we hypothesize that LLR may be a more accurate dissimilarity metric for groupwise registration than GLR.

Based on these motivations, we propose a deformable groupwise registration method based on an LLR dissimilarity metric and validate its performance for the estimation of myocardial strains. A variety of alternative methods were compared, including optical flow, pairwise registration, and GLR-based groupwise registration over criteria such as myocardial tracking accuracy, strain accuracy, and strain reproducibility. The comparison was performed on a digital cardiac phantom (XCAT)[23] and a public in vivo dataset (ACDC)[24]. A preliminary version of this work has been reported as an abstract in the 2023 ISMRM Annual Meeting[25].

II. METHODS

A. Groupwise registration

1) Transformation model

The goal of groupwise registration is to simultaneously align all cine images to a common reference frame. Let $f(\mathbf{x}, t)$ represent the cine image sequence, where $\mathbf{x} \in \Omega = \{(x, y) | 1 \leq x \leq N_x, 1 \leq y \leq N_y\}$ and $1 \leq t \leq N_t$. The deformed cine image sequence can be expressed as

$$\tilde{f}(\mathbf{x}, t) = f(\mathbf{T}(\mathbf{x}, t), t) = f(\mathbf{x} + \mathbf{d}(\mathbf{x}, t), t), \quad (1)$$

where $\mathbf{T}(\mathbf{x}, t) = \mathbf{x} + \mathbf{d}(\mathbf{x}, t)$ is the transformation field, and $\mathbf{d}(\mathbf{x}, t)$ is the displacement field. We use the free-form deformation modeling of the displacement field[26]. Specifically, given a control point mesh $\boldsymbol{\phi}(i, j, t)$ with uniform control point spacing δ , $\mathbf{d}(\mathbf{x}, t)$ is modeled by a linear combination of control points with cubic B-spline coefficients as

$$\mathbf{d}(\mathbf{x}, t) = \sum_{k=0}^3 \sum_{l=0}^3 B_k(u) B_l(v) \boldsymbol{\phi}(i + k, j + l, t), \quad (2)$$

where $i = \lfloor (x - 1)/\delta \rfloor$, $j = \lfloor (y - 1)/\delta \rfloor$, $u = (x - 1)/\delta - \lfloor (x - 1)/\delta \rfloor$, $v = (y - 1)/\delta - \lfloor (y - 1)/\delta \rfloor$, and $B_k(u)$ is the k -th basis function of the B-splines. By constraining the temporal average of the transformation field to be an identity map or that of the displacement field to be zero, we register all images to an average common reference frame[27]:

$$\frac{1}{N_t} \sum_{t=1}^{N_t} \mathbf{T}(\mathbf{x}, t) = \mathbf{x} \Leftrightarrow \frac{1}{N_t} \sum_{t=1}^{N_t} \mathbf{d}(\mathbf{x}, t) = \mathbf{0}, \quad (3)$$

which based on (2) are equivalent to

$$\frac{1}{N_t} \sum_{t=1}^{N_t} \boldsymbol{\phi}(i, j, t) = \mathbf{0}. \quad (4)$$

2) Dissimilarity metrics

To introduce the LLR metric, we firstly review the GLR metric used in previous studies[16], [17]. Evaluation of GLR is initiated by reformulation of the deformed images into a global Casorati matrix:

$$\mathbf{C} = \begin{bmatrix} \tilde{f}(\mathbf{x}_1, 1) & \tilde{f}(\mathbf{x}_1, 2) & \cdots & \tilde{f}(\mathbf{x}_1, N_t) \\ \tilde{f}(\mathbf{x}_2, 1) & \tilde{f}(\mathbf{x}_2, 2) & \cdots & \tilde{f}(\mathbf{x}_2, N_t) \\ \vdots & \vdots & \ddots & \vdots \\ \tilde{f}(\mathbf{x}_L, 1) & \tilde{f}(\mathbf{x}_L, 2) & \cdots & \tilde{f}(\mathbf{x}_L, N_t) \end{bmatrix} \in \mathbb{R}^{L \times N_t}, \quad (5)$$

where $L = N_x N_y$ is the total number of voxels in the image. If the images are well aligned, the rows in the Casorati matrix are expected to be linearly dependent, or equivalently the matrix to be rank-deficient. The GLR dissimilarity is thus determined by the nuclear norm of \mathbf{C} :

$$D_{GLR} = \|\mathbf{C}\|_* = \sum_{t=1}^{rank(\mathbf{C})} \sigma_t, \quad (6)$$

where σ_t is the t -th singular value.

We now formulate the proposed LLR dissimilarity metric, which begins by a uniform partitioning of the image domain into a set of N_c patches with a prespecified patch size and spacing. The LLR dissimilarity is then determined by a sum of the nuclear norms from every patch:

$$D_{LLR} = \sum_{\kappa=1}^{N_c} \|\mathbf{C}_\kappa\|_*, \quad (7)$$

where \mathbf{C}_κ is the κ -th local Casorati matrix.

3) Regularization terms

We use a hybrid temporospatial regularization to improve the conditioning of the underlying optimization problem. For spatial smoothness of the transformation field, we use a bending-energy-based regularization[26]:

$$R_{spatial} = \sum_{t=1}^{N_t} \sum_{\mathbf{x} \in \Omega} \left\| \frac{\partial^2 \mathbf{T}}{\partial x^2}(\mathbf{x}, t) \right\|_2^2 + 2 \left\| \frac{\partial^2 \mathbf{T}}{\partial x \partial y}(\mathbf{x}, t) \right\|_2^2 + \left\| \frac{\partial^2 \mathbf{T}}{\partial y^2}(\mathbf{x}, t) \right\|_2^2. \quad (8)$$

For temporal smoothness of the transformation field, we use a regularization based on second-order finite differences:

$$R_{temporal} = \sum_{t=1}^{N_t} \sum_{\mathbf{x} \in \Omega} \left\| \frac{\partial^2 \mathbf{T}}{\partial t^2}(\mathbf{x}, t) \right\|_2^2. \quad (9)$$

Since cine image sequences are usually cyclic, $R_{temporal}$ can optionally adopt the cyclic finite difference to enforce the consistency of motion between the first and last images[28].

4) Optimization strategy

The resultant optimization problem of the LLR-based groupwise registration (Groupwise-LLR) is

$$\begin{aligned} \min_{\boldsymbol{\phi}} D_{LLR} + \lambda R_{spatial} + \mu R_{temporal} \\ \text{s. t. } \frac{1}{N_t} \sum_{t=1}^{N_t} \boldsymbol{\phi}(i, j, t) = \mathbf{0}, \end{aligned} \quad (10)$$

where λ and μ are the regularization coefficients. We propose to use the projected gradient algorithm[27] in a multiresolution manner[26] to solve the problem. Denoting the control point mesh in the n -th iteration as $\boldsymbol{\phi}^{(n)}$, the gradient as $\boldsymbol{g}^{(n)}$, and the step size as $\alpha^{(n)}$, the projected gradient algorithm executes the following update in each iteration (assuming $\boldsymbol{\phi}^{(0)} = \mathbf{0}$):

$$\boldsymbol{\phi}^{(n+1)} = \boldsymbol{\phi}^{(n)} - \alpha^{(n)}(\boldsymbol{g}^{(n)} - \frac{1}{N_t} \sum_{t=1}^{N_t} \boldsymbol{g}^{(n)}). \quad (11)$$

For evaluation of $\boldsymbol{g}^{(n)}$, note that the gradient of the nuclear norm $\|\mathbf{C}\|_*$ with respect to \mathbf{C} is approximated by $\mathbf{U}\mathbf{V}^T$, where \mathbf{U} and \mathbf{V} are the left and right singular vector matrices of \mathbf{C} , respectively.

B. Tracking and strain estimation

After we obtain the temporally resolved transformation field, we estimate the transformation field from the first image (end-diastole (ED)) to each later image by a two-step process[18], in which the coordinate \mathbf{x} in the ED image is firstly mapped to the common reference frame, and then to the t -th image. Mathematically, this process is represented by

$$\mathbf{T}_{1 \rightarrow t}(\mathbf{x}) = \mathbf{T}(\mathbf{T}^{-1}(\mathbf{x}, 1), t), \quad (12)$$

where $\mathbf{T}_{1 \rightarrow t}(\mathbf{x})$ represents the transformation field from the first image to the t -th image. Based on the estimated $\mathbf{T}_{1 \rightarrow t}(\mathbf{x})$, the Green-Lagrange strain tensor[29] is then evaluated by

$$\mathbf{E}(\mathbf{x}, t) = \frac{1}{2} \left[(\nabla_{\mathbf{x}} \mathbf{T}_{1 \rightarrow t}(\mathbf{x}))^T \nabla_{\mathbf{x}} \mathbf{T}_{1 \rightarrow t}(\mathbf{x}) - \mathbf{I} \right], \quad (13)$$

where $\nabla_{\mathbf{x}}$ represents the Jacobian operator about \mathbf{x} (implemented using finite differences) and \mathbf{I} is an identity matrix of size two. The strain along a certain direction is then given by

$$e_{\mathbf{u}}(\mathbf{x}, t) = (\mathbf{u}(\mathbf{x}))^T \mathbf{E}(\mathbf{x}, t) \mathbf{u}(\mathbf{x}), \quad (14)$$

where $\mathbf{u}(\mathbf{x})$ is the strain direction field determined by segmentation of the LV myocardium (LVM) in the ED image. For long-axis (LAX) slices, $\mathbf{u}(\mathbf{x})$ represents the longitudinal direction; for short-axis (SAX) slices, $\mathbf{u}(\mathbf{x})$ represents the circumferential or radial direction. The global longitudinal strain (GLS) is estimated by averaging the strain values within

a single long-axis slice. The global circumferential strain (GCS) and global radial strain (GRS) are estimated by averaging the strain values across multiple slices covering the entire LV.

C. Baseline methods

The proposed Groupwise-LLR was compared with the Farneback optical flow[30], a pairwise registration method[11], [31], [32], and the GLR-based groupwise registration (Groupwise-GLR). Among these methods, the optical flow and pairwise registration estimate the transformation field between each pair of the neighboring images, i.e., $\mathbf{T}_{t-1 \rightarrow t}(\mathbf{x})$, $2 \leq t \leq N_t$. The transformation field $\mathbf{T}_{1 \rightarrow t}(\mathbf{x})$ is then a composition of the neighboring transformation fields[11]. The Groupwise-GLR was implemented in the same way as Groupwise-LLR except for the use of GLR dissimilarity metric.

D. Implementation details

All methods were implemented with MATLAB (R2022a, MathWorks, Natick, MA, USA). The parameters of each method were manually tuned for the simulated and in vivo datasets. For the proposed Groupwise-LLR method, the number of resolution levels was 3, and the cine images were upsampled by a factor of 2 whenever the resolution was increased. The patch size and spacing used to sample the local Casorati matrices were 5 and 3 pixels at the lowest resolution level and doubled each time moving to the next level. The control point spacing, spatial regularization coefficient, and temporal regularization coefficient were 6 and 7 pixels, 6×10^{-4} and 1×10^{-3} , 0.06 and 0.1 for the simulated dataset and in vivo dataset, respectively. The optimization at each resolution level was terminated when the relative value change of the cost function was less than a tolerance of 1×10^{-6} or the maximal number of iterations 80 was reached.

III. EXPERIMENTS

A. Datasets

The simulated cine images were generated by a digital phantom (XCAT)[23] and its MRI extension MRXCAT[33]. Specifically, XCAT was used to generate the cardiac-phase-resolved 3D tissue masks of 20 subjects, each with a different gender, cardiac anatomy, and cardiac motion pattern. The corresponding transformation field was also generated for each subject. Interpolation was then used to generate 2D cine movies in 7 or 8 SAX slices and a 2-chamber slice, with a $1.5 \text{ mm} \times 1.5 \text{ mm}$ resolution and 24 frames. MRXCAT was used to generate the signal intensity of each tissue in cine MRI. Since the ground truth transformation field was available, we evaluated the ground truth longitudinal strain from the 2-chamber slice, and the ground truth circumferential and radial strains from the SAX slices.

In vivo evaluation was performed with the Automated Cardiac Diagnosis Challenge (ACDC) dataset[24], which includes annotated SAX cine movies from 100 subjects. These subjects are evenly distributed over five medical groups: dilated cardiomyopathy (DCM), myocardial infarction (MINF), abnormal right ventricle (ARV), hypertrophic cardiomyopathy (HCM), and normal cardiac anatomy and function (NOR). The

in-plane resolution ranges from 1.34 to 1.68 mm, through-plane resolution from 5 to 10 mm, and the number of frames from 28 to 40. Each cine movie covers either the entire cardiac cycle (retrospective gating) or the first 90-95% of the cardiac cycle (prospective gating). Manual segmentation of the ED and ES myocardium is provided by the dataset. Registration was performed to a 128×128 region of interest (ROI) covering the LV throughout the cardiac cycle. The signal values within the ROI were linearly normalized to $[0, 1]$. Only the SAX slices containing the LVM were kept for strain analysis.

B. Evaluation metrics

For the simulated dataset, tracking quality was evaluated by end-point errors (EPE). Among them, the end-systolic EPE is defined as

$$EPE_{ES} = \frac{1}{|\Omega_{ED,LVM}|} \sum_{\mathbf{x} \in \Omega_{ED,LVM}} \|\mathbf{T}_{1 \rightarrow t_{ES}}(\mathbf{x}) - \mathbf{T}_{1 \rightarrow t_{ES}}^{true}(\mathbf{x})\|_2, \quad (15)$$

and the average EPE over all time points is defined as

$$EPE_{all} = \frac{1}{|\Omega_{ED,LVM}|} \sum_{\mathbf{x} \in \Omega_{ED,LVM}} \left(\frac{1}{N_t} \sum_{t=1}^{N_t} \|\mathbf{T}_{1 \rightarrow t}(\mathbf{x}) - \mathbf{T}_{1 \rightarrow t}^{true}(\mathbf{x})\|_2 \right), \quad (16)$$

where $\mathbf{T}_{1 \rightarrow t}^{true}(\mathbf{x})$ is the ground truth transformation field, $\Omega_{ED,LVM}$ is the region of LVM at end-diastole, and $|\Omega_{ED,LVM}|$ is the number of voxels in $\Omega_{ED,LVM}$.

For the simulated dataset, the accuracy of strain estimates was evaluated at both voxelwise and global levels. The voxelwise strain accuracy was evaluated by an average of the end-systolic voxelwise strain error (VSE) over $\Omega_{ED,LVM}$, defined as

$$VSE_{ES} = \frac{1}{|\Omega_{ED,LVM}|} \sum_{\mathbf{x} \in \Omega_{ED,LVM}} |e_u(\mathbf{x}, t_{ES}) - e_u^{true}(\mathbf{x}, t_{ES})|, \quad (17)$$

where $e_u^{true}(\mathbf{x}, t_{ES})$ is the ground truth end-systolic strain. The global strain accuracy was evaluated by end-systolic global strain error (GSE), which is the absolute difference between the estimated global strain and its ground truth counterpart.

For the in vivo dataset, tracking quality was evaluated by mean distances between predictions and manual annotations of the end-systolic endocardial and epicardial contours. The predictions of these myocardial contours were generated by deforming the end-diastolic annotations of them according to the estimated transformation fields. Mathematically, the mean distance between two contours ∂A and ∂B is defined as

$$\text{Mean Dist.}(\partial A, \partial B) = \frac{1}{2|\partial A|} \sum_{\mathbf{x} \in \partial A} d(\mathbf{x}, \partial B) + \frac{1}{2|\partial B|} \sum_{\mathbf{x} \in \partial B} d(\mathbf{x}, \partial A), \quad (18)$$

where $|\partial A|$ is the number of pixels in ∂A , and $d(\mathbf{x}, \partial A)$ is the minimal distance from the point \mathbf{x} to ∂A . This is an indirect measure of tracking quality used also by other studies[34], [35] when the ground truth transformation field was unknown. For

each subject, the basal, mid-ventricular, and apical slices were used to evaluate the mean contour distances.

For the in vivo dataset, voxelwise strain maps were generated for each registration method over the 100 subjects. Only GCS and GRS at each cardiac phase were evaluated since LAX slices were not provided. To evaluate inter-observer reproducibility, the myocardium in the ED images of 30 subjects (6 subjects from each group) was also segmented by another observer (HC, 3 years of cardiac MR experience). GCS and GRS were evaluated again using the new segmentations. The inter-observer reproducibility was then assessed by intraclass correlation (ICC) and Bland-Altman analyses.

C. Statistical analysis

Continuous variables were reported as mean \pm standard deviation. The paired-sample t-test was performed for comparisons of continuous variables. ICC was evaluated using a single rating, absolute agreement, and 2-way mixed-effects model[36]. The statistical analyses were performed with MATLAB (R2022a, MathWorks, Natick, MA, USA) and SPSS (Version 26, IBM, New York, USA). A p value less than 0.05 was considered statistically significant.

IV. RESULTS

A. Illustration of LLR's advantage

Fig. 1 shows the decrease of LLR costs after registration to illustrate the incremental value of LLR over GLR. For a fair comparison, the registration was accomplished by Groupwise-GLR, and the registration quality was visually verified to be good. The first row shows the LLR costs for different patch sizes before the registration, the second row shows them after the registration, and the third row shows the relative difference between the first and second rows. When the patch size is small, the reduction of the LLR cost through the registration is region-dependent. For regions where no myocardial motion is involved,

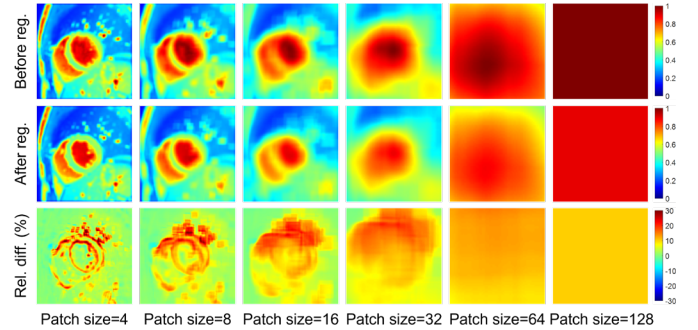


Fig. 1. LLR cost maps of a cine image sequence before (Row 1) and after (Row 2) registration. Row 3 shows the relative difference between Row 1 and Row 2, which informs about the spatially varying reduction of the LLR cost after registration. When the patch size for evaluating LLR is small, the reduction of LLR cost is region-dependent, with higher reductions in regions with more intense motion, such as the myocardial borders. When the patch size is large, the reduction of LLR cost becomes less region-dependent. When the patch size equals 128, which is the size of the image, LLR is equivalent to GLR. In this case, the reduction of LLR or GLR cost is spatially uniform and considerably smaller ($\sim 10\%$) than the maximal reduction of the LLR cost with a small patch size ($\sim 40\%$). The difference between LLR and GLR indicates that LLR can better distinguish between regions of different motion intensities than GLR, and thus may facilitate more targeted registration of the underlying movement.

the reduction of LLR cost is low. For regions where myocardial motion is intense, such as the myocardial borders, the reduction of LLR cost is as high as about 40%. Minimization of the LLR cost will thus focus on these motion-intense regions, resulting in a region-informed registration. On the other hand, note that the LLR with a patch size of 128×128 (the rightmost column) is essentially GLR. Compared with the heterogeneous reductions of the LLR cost, the reduction of GLR cost is about 10% for the entire image. The lack of reduction is because incoherent signal variations exist even after the registration, such as the transient flow signals in the blood pool. The evaluation of GLR ignores the spatial heterogeneity of signal variations and thus may lack sensitivity to regions of intense motions.

B. Simulated dataset

Fig. 2 shows changes of the EPE, VSE, and global strains over the entire cardiac cycle for one simulated subject. Groupwise-LLR achieved substantially lower errors for tracking and strain estimation over the entire cardiac cycle. The largest improvement was found at end-systole (orange arrows),

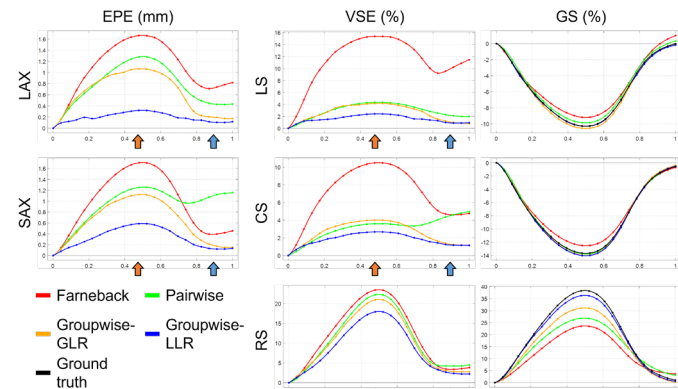


Fig. 2. Plots of the EPE, VSE, and global strains over a cardiac cycle for one simulated subject. The curves were plotted as a function of normalized time. Groupwise-LLR achieved the lowest errors among the four methods for tracking, voxelwise strain estimation, and global strain estimation. The largest improvement occurred at end-systole (orange arrows). In late-diastole, the two groupwise methods were more accurate than Farneback optical flow and pairwise registration (blue arrows) due to the elimination of the drift effect. (EPE: end-point error; VSE: voxelwise strain error; GS: global strain; LAX: long-axis; SAX: short-axis; LS: longitudinal strain; CS: circumferential strain; RS: radial strain)

where Groupwise-LLR was better than Groupwise-GLR and pairwise registration, both of which were better than Farneback optical flow. In late-diastole (blue arrows), the groupwise methods were more accurate than pairwise registration and Farneback, both of which suffered from the drift effect. Groupwise-LLR had the most similar global strains compared with the ground truth. Particularly, Groupwise-LLR generated a substantially more accurate radial strain than the other methods.

Fig. 3 shows the end-systolic strain maps obtained from the four methods and ground truth for the same subject in Figure 1. Farneback optical flow generated spurious discontinuities and errors in the estimated strain (black arrowheads). Pairwise registration was better than Farneback optical flow, but it still underestimated the longitudinal and radial strain (red arrowheads). Groupwise-GLR and Groupwise-LLR led to more accurate strains than the previous two methods. Furthermore, Groupwise-LLR yielded a more accurate radial strain than Groupwise-GLR (green arrowheads).

Table I compares the values of EPE_{ES} , EPE_{all} , VSE_{ES} , and GSE_{ES} from the four methods over all simulated subjects. Groupwise-LLR achieved significantly lower EPE_{ES} and EPE_{all}

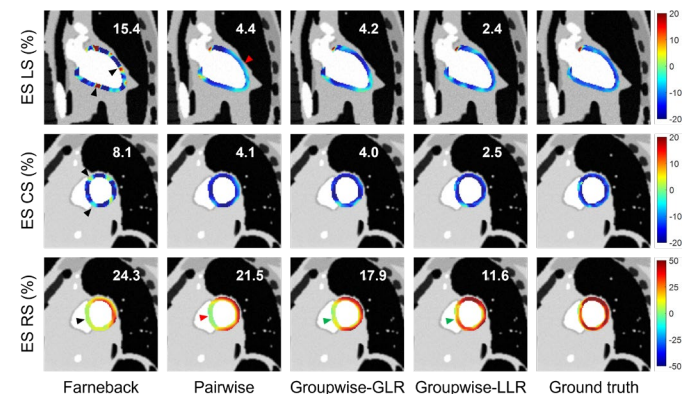


Fig. 3. ES strain maps of the same subject in Fig. 2 generated from different methods and the ground truth. Rows 1, 2, and 3 showed the ES LS, CS, and RS, respectively. The VSE (%) of one slice is labeled at the top of each image. Farneback optical flow caused nonsmooth and inaccurate strain estimates (black arrows). Pairwise registration underestimated LS and RS in several myocardial segments (red arrows). Groupwise-LLR showed more accurate estimates of RS than Groupwise-GLR (green arrows). Moreover, Groupwise-LLR achieved the lowest VSE among the four methods. (ES: end-systolic; LS: longitudinal strain; CS: circumferential strain; RS: radial strain)

TABLE I
COMPARISON OF THE END-POINT ERRORS, VOXELWISE STRAIN ERRORS, AND GLOBAL STRAIN ERRORS BETWEEN DIFFERENT METHODS.

Method	EPE_{ES} (mm)		EPE_{all} (mm)		VSE_{ES} (%)			GSE_{ES} (%)		
	LAX	SAX	LAX	SAX	LS	CS	RS	LS	CS	RS
Farneback	1.36	1.46	0.82	0.80	10.23	9.14	19.83	0.99	1.03	8.70
	$\pm 0.47^*$	$\pm 0.29^*$	$\pm 0.29^*$	$\pm 0.18^*$	$\pm 3.50^*$	$\pm 1.48^*$	$\pm 5.35^*$	$\pm 0.70^*$	$\pm 0.84^*$	$\pm 5.36^*$
Pairwise	1.07	0.97	0.64	0.68	3.40	3.21	15.73	0.84	0.34	6.17
	$\pm 0.46^*$	$\pm 0.18^*$	$\pm 0.23^*$	$\pm 0.13^*$	$\pm 0.84^*$	$\pm 0.65^*$	$\pm 4.47^*$	$\pm 0.52^*$	$\pm 0.24^*$	$\pm 4.00^*$
Groupwise-GLR	0.88	0.95	0.49	0.53	3.68	3.88	15.55	0.38	0.31	4.02
	$\pm 0.34^*$	$\pm 0.21^*$	$\pm 0.17^*$	$\pm 0.13^*$	$\pm 0.97^*$	$\pm 0.64^*$	$\pm 4.23^*$	$\pm 0.25^*$	$\pm 0.23^*$	$\pm 3.09^*$
Groupwise-LLR	0.37	0.48	0.22	0.27	2.19	2.61	12.80	0.20	0.21	1.66
	± 0.11	± 0.13	± 0.06	± 0.08	± 0.46	± 0.57	± 3.82	± 0.21	± 0.14	± 1.15

*: Significantly higher error than Groupwise-LLR based on one-tailed paired t-test. (EPE: end-point error; VSE: voxelwise strain error; GSE: global strain error; ES: end-systolic; LAX: long-axis; SAX: short-axis; LS: longitudinal strain; CS: circumferential strain; RS: radial strain)

compared with all three other methods for both LAX and SAX views, suggesting that Groupwise-LLR achieved better tracking accuracy. Furthermore, Groupwise-LLR achieved significantly lower VSE_{ES} and GSE_{ES} than the other three methods for all strain types. The result implies that Groupwise-LLR generates more accurate strains at both global and voxelwise levels. In particular, Groupwise-LLR led to dramatically reduced errors for the global radial strain.

C. In vivo dataset

Fig. 4 compares the tracking quality of the four methods, measured by the mean distance between each predicted contour and manually drawn contour at end-systole. For both epicardial and endocardial contours, Groupwise-LLR achieved significantly lower mean distances ($1.75 \text{ mm} \pm 0.65 \text{ mm}$ and $2.12 \text{ mm} \pm 1.40 \text{ mm}$) than Farneback optical flow ($1.88 \text{ mm} \pm 0.72 \text{ mm}$, $p=0.000$, and $2.50 \text{ mm} \pm 1.61 \text{ mm}$, $p=0.000$), pairwise registration ($1.80 \text{ mm} \pm 0.72 \text{ mm}$, $p=0.004$, and $2.30 \text{ mm} \pm 1.47 \text{ mm}$, $p=0.000$) and Groupwise-GLR ($1.85 \text{ mm} \pm 0.73 \text{ mm}$, $p=0.000$, and $2.17 \text{ mm} \pm 1.48 \text{ mm}$, $p=0.019$) based on one-sided paired-sample t-test. These results suggest that Groupwise-LLR had a superior in vivo tracking quality than the other three methods.

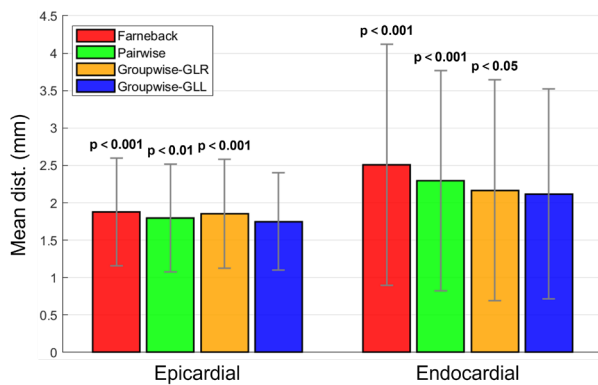


Fig. 4. Comparison of the tracking quality of different methods for the in vivo dataset. The height of each bar represents the mean value of the mean distance between the predicted contour by each registration method and manually drawn contour at end-systole. The error bar indicates the standard deviation. For each subject, only the basal, mid-ventricular, and apical slices were used for the contour tracking. The p value from one-sided paired-sample t-test is labeled over each bar for the three alternative methods. Groupwise-LLR showed a significant reduction of mean distance compared with the other methods for both the epicardial and endocardial contours.

Fig. 5 shows the global strain curves of three subjects, each from a different medical group. For every method, the MINF and DCM subjects had lower strains than the normal control. Note that the two groupwise methods generated strains closer to zero at late-diastole, which is correct due to the motion periodicity, whereas the two pairwise methods often generated nonzero strains at late-diastole due to the drift effect (arrows). Fig. 6 shows the mid-ventricular strain maps obtained by different methods for a MINF subject, who has wall thinning and akinesia in the septum (cf. Supporting Information Movie S1). All four methods captured the reduction of radial strain in the septum; however, Farneback also showed lower radial strain in the anterior wall, which was not accurate and not found with the other methods. Furthermore, the two groupwise methods

generated more accurate strain estimates in the last image due to the elimination of the drift effect.

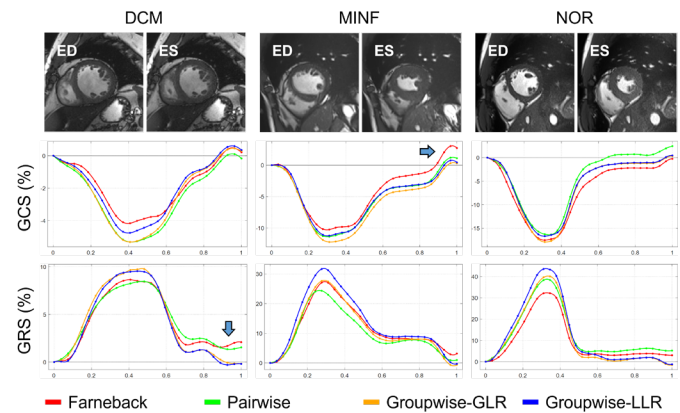


Fig. 5. Global circumferential and radial strain curves of three subjects from different medical groups. The curves were plotted as a function of normalized time. The ED and ES mid-ventricular images of each subject are shown at the top of each column. Normally, the strain at the end of the cardiac cycle should be nearly zero due to the quasi-periodicity of the cine image sequences. However, in the presence of the drift effect, the late-diastolic strain can be significantly different from zero, which is observed for the Farneback optical flow and pairwise registration method but not for the groupwise methods. (DCM: dilated cardiomyopathy; MINF: myocardial infarction; NOR: normal cardiac anatomy and function; ED: end-diastolic; ES: end-systolic; GCS: global circumferential strain; GRS: global radial strain)

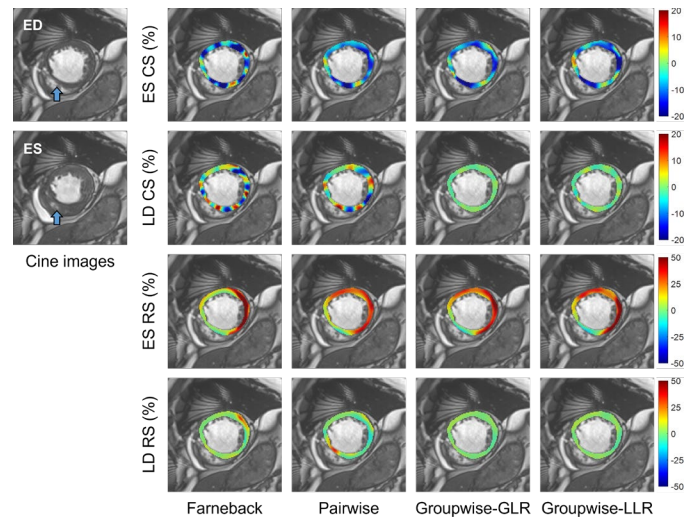


Fig. 6. Mid-ventricular cine images of one subject with myocardial infarction and the corresponding end-systolic and late-diastolic CS and RS maps. The septal wall (arrows) exhibited abnormal thinning and akinesia due to the presence of infarction. Farneback caused nonsmooth estimates of CS and underestimates of RS in the anterior wall. Both Farneback and pairwise registration suffered from the drift effect and manifested nonzero strains in the late-diastolic image. The groupwise registration methods demonstrated a smoother circumferential strain map, more accurate RS estimates, and elimination of the drift effect. (ED: end-diastolic; ES: end-systolic; LD: late-diastolic (corresponding to the last cine image); CS: circumferential strain; RS: radial strain)

Fig. 7 shows the mean and 95% confidence interval of the global strain curves over each medical group obtained by different methods. One can notice the systematic occurrence of drift effects in late-diastole with the two pairwise methods. In addition, Farneback optical flow seemed to generate more inconsistent strain estimates compared with the other three methods. For example, the average peak GRS of the HCM

group was higher than that of the control group in the Farneback measurement, whereas the opposite trend was found with the other three methods.

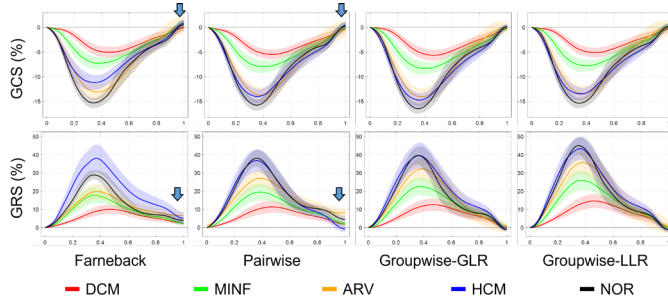


Fig. 7. The mean and confidence interval of the global circumferential and radial strain curves over each medical group (n=20). Each curve represents an average global strain, with different colors representing different medical groups. The shade around each curve represents the 95% confidence interval at each time point. The arrows highlight the systematic drift effect of Farneback optical flow and pairwise registration. (GCS: global circumferential strain; GRS: global radial strain; DCM: dilated cardiomyopathy; MINF: myocardial infarction; ARV: abnormal right ventricle; HCM: hypertrophic cardiomyopathy; NOR: normal cardiac anatomy and function)

Table II shows the ES global strains obtained by different methods for each medical group. Groupwise-LLR generated a significantly greater GRS for every medical group than the other methods, whereas the GCS was more similar. These trends were consistent with the findings from the simulated dataset.

Fig. 8 shows the Bland-Altman analysis of inter-observer reproducibility for each method. Overall, all four methods had a similar inter-observer reproducibility. ICC and its 95% confidence interval were labeled at the top of each plot. For each method, the ICC of GCS was “moderate” to “excellent”, while that of GRS was “excellent” [36]. Hence, the reproducibility of radial strain seems to be better than that of circumferential strain for all methods.

V. DISCUSSION

In this work, we propose a deformable groupwise registration method using an LLR dissimilarity metric to estimate myocardial strains from cardiac cine MRI images. We evaluated the tracking accuracy, strain accuracy, and strain

TABLE II
COMPARISON OF THE END-SYSTOLIC GLOBAL CIRCUMFERENTIAL AND RADIAL STRAINS BETWEEN DIFFERENT METHODS.

Method	ES GCS (%)					ES GRS (%)				
	DCM	MINF	ARV	HCM	NOR	DCM	MINF	ARV	HCM	NOR
Farneback	-5.2 ±2.4	-7.6 ±2.4*	-13.8 ±3.2	-11.3 ±3.2*	-15.8 ±2.0	9.8 ±5.1*	19.6 ±8.4*	21.7 ±7.9*	38.6 ±16.5*	31.1 ±6.0*
Pairwise	-5.6 ±2.1*	-8.4 ±2.6	-14.5 ±2.6	-14.2 ±3.2	-16.2 ±2.2	11.1 ±6.6*	21.2 ±8.7*	29.7 ±9.1*	37.5 ±13.2*	39.8 ±10.3*
Groupwise-GLR	-5.7 ±2.3*	-8.7 ±2.7*	-14.8 ±3.2*	-14.9 ±3.0*	-17.0 ±1.8*	12.5 ±7.0*	24.9 ±9.4*	35.5 ±11.6*	40.0 ±15.3*	41.8 ±10.8*
Groupwise-LLR	-5.1 ±2.1	-8.2 ±2.4	-14.2 ±2.8	-13.6 ±2.7	-15.9 ±2.0	14.5 ±7.7	28.8 ±9.2	39.3 ±11.7	43.8 ±13.2	47.8 ±11.8

*: significantly different from the strain estimated by Groupwise-LLR according to the two-tailed paired t-test. (ES: end-systolic; GCS: global circumferential strain; GRS: global radial strain; DCM: dilated cardiomyopathy; MINF: myocardial infarction; ARV: abnormal right ventricle; HCM: hypertrophic cardiomyopathy; NOR: normal cardiac anatomy and function)

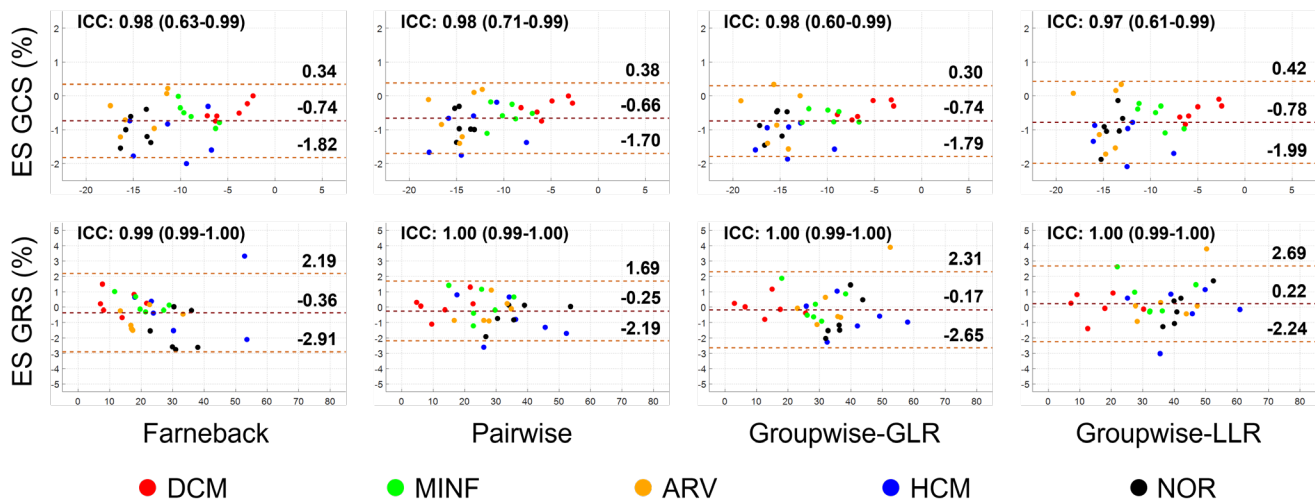


Fig. 8. Evaluation of inter-observer reproducibility of end-systolic global strains by Bland-Altman analysis. Overall, all four methods had a similar inter-observer reproducibility. The disagreement of GCS was greater than that of GRS for every method. ICC and its 95% confidence interval are labeled at the top of each plot. (ES: end-systolic; GCS: global circumferential strain; GRS: global radial strain; ICC: intraclass correlation coefficient; DCM: dilated cardiomyopathy; MINF: myocardial infarction; ARV: abnormal right ventricle; HCM: hypertrophic cardiomyopathy; NOR: normal cardiac anatomy and function)

inter-observer reproducibility of the proposed method via simulated and in vivo data. Our major finding is that Groupwise-LLR generated more accurate tracking compared with previous methods, and more accurate strain estimates in late-diastole. The simulated dataset also confirmed more accurate strains over the entire cardiac cycle with Groupwise-LLR. The in vivo data showed a similar inter-observer reproducibility among all four methods.

Although tagging-MRI is the gold standard for strain measurement, it requires the application of a separate sequence and complicated post-processing[37]. Feature tracking based on cine images does not require other sequences and is relatively easy to post-process. For the becoming a more popular method for myocardial strain estimation[38]–[40]. Optical flow is currently the major algorithm used in existing commercial software for feature tracking. However, the CMR-FT methods based on optical flow can be sensitive to noise and artifacts since they highly rely on local textures, which are however scarce in the myocardial regions of cine MRI images[19]. Consistent with previous findings, our results also indicated that the strains estimated by Farneback optical flow were spatially nonsmooth and less accurate at a regional level. Pairwise registration is used by a more recent commercial software Segment CMR (Medviso, Lund, Sweden) for FT-based strain estimation and has been compared to optical flow-based methods[6], [41]. However, since all of them are pairwise alignment methods, they are susceptible to the drift effect, which generates inaccurate strains, especially for late-diastole[5], [10]. Although groupwise registration has been validated for myocardial tracking[18], [19], it has not been validated as a strain estimation method. Our findings echoed the overall impression that groupwise registration yields more accurate strain estimates. Furthermore, due to the improved discrimination of local signal variations, the proposed Groupwise-LLR method showed improved myocardial tracking accuracy relative to the Groupwise-GLR method. Groupwise-LLR may thus allow more accurate strain estimates compared to current FT methods.

The proposed LLR dissimilarity metric can also be used for other tasks where groupwise registration is needed. For example, cardiac MRI parametric mapping acquires multiple T1 or T2 weighted images over multiple heartbeats, for which motion often occurs across different heartbeats[42]. The proposed method can be used to correct motion in this task since the aligned images should have a lower rank in each local region. Other non-medical tasks, such as multi-exposure image fusion[43], [44] and video stabilization[45], [46] also face spatially varying signal dynamics even after image alignment. The proposed Groupwise-LLR method may find applications in these scenarios as well.

The study has several limitations. Firstly, the longitudinal strain was not validated on the in vivo images, since long-axis images were not provided by the ACDC dataset. However, the results on the simulated dataset preliminarily validated the potential of the proposed method for longitudinal strain estimation. Secondly, we did not compare our method with the gold standard method for in vivo strain estimation, such as

tagging-MRI. The accuracy of in vivo strain estimation thus needs to be further investigated. Finally, we only validated our method using a relatively small and diverse patient cohort. Further studies based on a larger patient cohort for evaluation of strain abnormality of a certain disease are highly warranted.

VI. CONCLUSION

In conclusion, we developed a deformable groupwise registration method based on a novel LLR dissimilarity metric for cine-MRI-based myocardial strain estimation. Our results based on simulated and in vivo datasets suggest that the method improves the accuracy of myocardial tracking and strain estimation compared with previous methods, due to the elimination of the drift effect and finer modeling of spatial low-rankness. The proposed method may generate more accurate strain estimates to improve quantitative assessments and diagnosis of cardiovascular diseases.

REFERENCES

- [1] O. A. Smiseth, H. Torp, A. Opdahl, K. H. Haugaa, and S. Urheim, "Myocardial strain imaging: how useful is it in clinical decision making?," *Eur Heart J*, vol. 37, no. 15, pp. 1196–1207, Apr. 2016, doi: 10.1093/eurheartj/ehv529.
- [2] M. S. Amzulescu *et al.*, "Myocardial strain imaging: review of general principles, validation, and sources of discrepancies," *European Heart Journal - Cardiovascular Imaging*, vol. 20, no. 6, pp. 605–619, Jun. 2019, doi: 10.1093/ehjci/jez041.
- [3] L. Wu, T. Germans, A. Güçlü, M. W. Heymans, C. P. Allaart, and A. C. van Rossum, "Feature tracking compared with tissue tagging measurements of segmental strain by cardiovascular magnetic resonance," *Journal of Cardiovascular Magnetic Resonance*, vol. 16, no. 1, p. 10, Jan. 2014, doi: 10.1186/1532-429X-16-10.
- [4] W. E. Moody *et al.*, "Comparison of magnetic resonance feature tracking for systolic and diastolic strain and strain rate calculation with spatial modulation of magnetization imaging analysis," *Journal of Magnetic Resonance Imaging*, vol. 41, no. 4, pp. 1000–1012, 2015, doi: 10.1002/jmri.24623.
- [5] C. Tobon-Gomez *et al.*, "Benchmarking framework for myocardial tracking and deformation algorithms: An open access database," *Medical Image Analysis*, vol. 17, no. 6, pp. 632–648, Aug. 2013, doi: 10.1016/j.media.2013.03.008.
- [6] M. Barreiro-Pérez, D. Curione, R. Symons, P. Claus, J.-U. Voigt, and J. Bogaert, "Left ventricular global myocardial strain assessment comparing the reproducibility of four commercially available CMR-feature tracking algorithms," *Eur Radiol*, vol. 28, no. 12, pp. 5137–5147, Dec. 2018, doi: 10.1007/s00330-018-5538-4.
- [7] M. A. Morales *et al.*, "DeepStrain: a deep learning workflow for the automated characterization of cardiac mechanics," *Frontiers in Cardiovascular Medicine*, p. 1041, 2021.
- [8] K. K. Bhatia, J. V. Hajnal, B. K. Puri, A. D. Edwards, and D. Rueckert, "Consistent groupwise non-rigid registration for atlas construction," in *2004 2nd IEEE International Symposium on Biomedical Imaging: Macro to Nano (IEEE Cat No. 04EX821)*, Arlington, VA, USA: IEEE, 2004, pp. 908–911. doi: 10.1109/ISBI.2004.1398686.
- [9] M. Ye *et al.*, "DeepTag: An Unsupervised Deep Learning Method for Motion Tracking on Cardiac Tagging Magnetic Resonance Images." arXiv, Apr. 18, 2021. Accessed: Sep. 25, 2022. [Online]. Available: <http://arxiv.org/abs/2103.02772>
- [10] M. De Craene *et al.*, "Temporal Diffeomorphic Free Form Deformation (TDFD) Applied to Motion and Deformation Quantification of Tagged MRI Sequences," in *Statistical Atlases and Computational Models of the Heart. Imaging and Modelling Challenges*, O. Camara, E. Konukoglu, M. Pop, K. Rhode, M. Sermesant, and A. Young, Eds., in Lecture Notes in Computer Science. Berlin, Heidelberg: Springer, 2012, pp. 68–77. doi: 10.1007/978-3-642-28326-0_7.
- [11] B. Heyde *et al.*, "Elastic Image Registration to Quantify 3-D Regional Myocardial Deformation from Volumetric Ultrasound: Experimental

- Validation in an Animal Model,” *Ultrasound in Medicine & Biology*, vol. 39, no. 9, pp. 1688–1697, Sep. 2013, doi: 10.1016/j.ultrasmedbio.2013.02.463.
- [12] J.-U. Voigt *et al.*, “Definitions for a Common Standard for 2D Speckle Tracking Echocardiography: Consensus Document of the EACVI/ASE/Industry Task Force to Standardize Deformation Imaging,” *Journal of the American Society of Echocardiography*, vol. 28, no. 2, pp. 183–193, Feb. 2015, doi: 10.1016/j.echo.2014.11.003.
- [13] K. K. Bhatia, J. Hajnal, A. Hammers, and D. Rueckert, “Similarity Metrics for Groupwise Non-rigid Registration,” in *Medical Image Computing and Computer-Assisted Intervention – MICCAI 2007*, N. Ayache, S. Ourselin, and A. Maeder, Eds., in Lecture Notes in Computer Science, vol. 4792. Berlin, Heidelberg: Springer Berlin Heidelberg, 2007, pp. 544–552. doi: 10.1007/978-3-540-75759-7_66.
- [14] S. K. Balci, P. Golland, M. Shenton, and W. M. Wells, “Free-Form B-spline Deformation Model for Groupwise Registration,” 2010.
- [15] W. Huiying *et al.*, “PCA-based groupwise image registration for quantitative MRI,” *Medical Image Analysis*, vol. 29, pp. 65–78, Apr. 2016, doi: 10.1016/j.media.2015.12.004.
- [16] Y. Peng, A. Ganesh, J. Wright, W. Xu, and Y. Ma, “RASL: Robust Alignment by Sparse and Low-Rank Decomposition for Linearly Correlated Images,” *IEEE Transactions on Pattern Analysis and Machine Intelligence*, vol. 34, no. 11, pp. 2233–2246, Nov. 2012, doi: 10.1109/TPAMI.2011.282.
- [17] R. Haase, S. Heldmann, and J. Lellmann, “Deformable groupwise image registration using low-rank and sparse decomposition,” *Journal of Mathematical Imaging and Vision*, vol. 64, no. 2, pp. 194–211, 2022.
- [18] C. T. Metz, S. Klein, M. Schaap, T. Van Walsum, and W. J. Niessen, “Nonrigid registration of dynamic medical imaging data using nD+t B-splines and a groupwise optimization approach,” *Medical Image Analysis*, vol. 15, no. 2, pp. 238–249, Apr. 2011, doi: 10.1016/j.media.2010.10.003.
- [19] M. Qiao, Y. Wang, Y. Guo, L. Huang, L. Xia, and Q. Tao, “Temporally coherent cardiac motion tracking from cine MRI: Traditional registration method and modern CNN method,” *Med Phys*, vol. 47, no. 9, pp. 4189–4198, Sep. 2020, doi: 10.1002/mp.14341.
- [20] T. Zhang, J. M. Pauly, and I. R. Levesque, “Accelerating parameter mapping with a locally low rank constraint: Locally Low Rank Parameter Mapping,” *Magn. Reson. Med.*, vol. 73, no. 2, pp. 655–661, Feb. 2015, doi: 10.1002/mrm.25161.
- [21] X. Miao *et al.*, “Accelerated cardiac cine MRI using locally low rank and finite difference constraints,” *Magnetic Resonance Imaging*, vol. 34, no. 6, pp. 707–714, Jul. 2016, doi: 10.1016/j.mri.2016.03.007.
- [22] Y. Peng, A. Ganesh, J. Wright, W. Xu, and Y. Ma, “RASL: Robust Alignment by Sparse and Low-rank Decomposition for Linearly Correlated Images,” 2011.
- [23] W. P. Segars, G. Sturgeon, S. Mendonca, J. Grimes, and B. M. W. Tsui, “4D XCAT phantom for multimodality imaging research,” *Medical Physics*, vol. 37, no. 9, pp. 4902–4915, 2010, doi: 10.1118/1.3480985.
- [24] O. Bernard *et al.*, “Deep Learning Techniques for Automatic MRI Cardiac Multi-Structures Segmentation and Diagnosis: Is the Problem Solved?,” *IEEE Trans. Med. Imaging*, vol. 37, no. 11, pp. 2514–2525, Nov. 2018, doi: 10.1109/TMI.2018.2837502.
- [25] H. Chen and C. Hu, “Deformable Groupwise Registration Using a Locally Low-Rank Dissimilarity for Myocardial Strain Estimation from Cine MRI Images,” *The International Society for Magnetic Resonance in Medicine (ISMRM) Annual Meeting*, 2023.
- [26] D. Rueckert, L. I. Sonoda, C. Hayes, D. L. Hill, M. O. Leach, and D. J. Hawkes, “Nonrigid registration using free-form deformations: application to breast MR images,” *IEEE transactions on medical imaging*, vol. 18, no. 8, pp. 712–721, 1999.
- [27] K. K. Bhatia, J. V. Hajnal, B. K. Puri, A. D. Edwards, and D. Rueckert, “Consistent groupwise non-rigid registration for atlas construction,” in *2004 2nd IEEE International Symposium on Biomedical Imaging: Nano to Macro (IEEE Cat No. 04EX821)*, IEEE, 2004, pp. 908–911.
- [28] J. Royuela-del-Val, L. Cordero-Grande, F. Simmross-Wattenberg, M. Martín-Fernández, and C. Alberola-López, “Nonrigid groupwise registration for motion estimation and compensation in compressed sensing reconstruction of breath-hold cardiac cine MRI,” *Magn Reson Med*, vol. 75, no. 4, pp. 1525–1536, Apr. 2016, doi: 10.1002/mrm.25733.
- [29] W. M. Lai, D. Rubin, and E. Krempl, *Introduction to continuum mechanics*, 4th ed. Amsterdam ; Boston: Butterworth-Heinemann/Elsevier, 2010.
- [30] G. Farné, “Two-Frame Motion Estimation Based on Polynomial Expansion,” in *Image Analysis*, J. Bigun and T. Gustavsson, Eds., in Lecture Notes in Computer Science, vol. 2749. Berlin, Heidelberg: Springer Berlin Heidelberg, 2003, pp. 363–370. doi: 10.1007/3-540-45103-X_50.
- [31] P. Morais, B. Heyde, D. Barbosa, S. Queirós, P. Claus, and J. D’hooge, “Cardiac Motion and Deformation Estimation from Tagged MRI Sequences Using a Temporal Coherent Image Registration Framework,” in *Functional Imaging and Modeling of the Heart*, S. Ourselin, D. Rueckert, and N. Smith, Eds., in Lecture Notes in Computer Science, vol. 7945. Berlin, Heidelberg: Springer Berlin Heidelberg, 2013, pp. 316–324. doi: 10.1007/978-3-642-38899-6_38.
- [32] P. Morais *et al.*, “Cardiovascular magnetic resonance myocardial feature tracking using a non-rigid, elastic image registration algorithm: assessment of variability in a real-life clinical setting,” *J Cardiovasc Magn Reson*, vol. 19, no. 1, p. 24, Dec. 2017, doi: 10.1186/s12968-017-0333-y.
- [33] L. Wissmann, C. Santelli, W. P. Segars, and S. Kozierke, “MRXCAT: Realistic numerical phantoms for cardiovascular magnetic resonance,” *Journal of Cardiovascular Magnetic Resonance*, vol. 16, no. 1, p. 63, Aug. 2014, doi: 10.1186/s12968-014-0063-3.
- [34] H. Xue *et al.*, “Motion correction for myocardial T1 mapping using image registration with synthetic image estimation,” *Magnetic resonance in medicine*, vol. 67, no. 6, pp. 1644–1655, 2012.
- [35] S. Roujol *et al.*, “Impact of motion correction on reproducibility and spatial variability of quantitative myocardial T2 mapping,” *J Cardiovasc Magn Reson*, vol. 17, no. 1, p. 46, Jun. 2015, doi: 10.1186/s12968-015-0141-1.
- [36] T. K. Koo and M. Y. Li, “A Guideline of Selecting and Reporting Intraclass Correlation Coefficients for Reliability Research,” *J Chiropr Med*, vol. 15, no. 2, pp. 155–163, Jun. 2016, doi: 10.1016/j.jcm.2016.02.012.
- [37] E.-S. H. Ibrahim, “Myocardial tagging by Cardiovascular Magnetic Resonance: evolution of techniques—pulse sequences, analysis algorithms, and applications,” *J Cardiovasc Magn Reson*, vol. 13, no. 1, p. 36, Dec. 2011, doi: 10.1186/1532-429X-13-36.
- [38] T. Pandey *et al.*, “Evaluation of Myocardial Strain in Patients With Amyloidosis Using Cardiac Magnetic Resonance Feature Tracking,” *Current Problems in Diagnostic Radiology*, vol. 46, no. 4, pp. 288–294, Jul. 2017, doi: 10.1067/j.cpradiol.2016.11.008.
- [39] J. A. Luetkens *et al.*, “Feature-tracking myocardial strain analysis in acute myocarditis: diagnostic value and association with myocardial oedema,” *Eur Radiol*, vol. 27, no. 11, pp. 4661–4671, Nov. 2017, doi: 10.1007/s00330-017-4854-4.
- [40] J. Xu, W. Yang, S. Zhao, and M. Lu, “State-of-the-art myocardial strain by CMR feature tracking: clinical applications and future perspectives,” *Eur Radiol*, vol. 32, no. 8, pp. 5424–5435, Aug. 2022, doi: 10.1007/s00330-022-08629-2.
- [41] S. Militaru *et al.*, “Multivendor comparison of global and regional 2D cardiovascular magnetic resonance feature tracking strains vs tissue tagging at 3T,” *Journal of Cardiovascular Magnetic Resonance*, vol. 23, no. 1, p. 54, May 2021, doi: 10.1186/s12968-021-00742-3.
- [42] P. K. Kim *et al.*, “Myocardial T1 and T2 Mapping: Techniques and Clinical Applications,” *Korean Journal of Radiology*, vol. 18, no. 1, pp. 113–131, Feb. 2017, doi: 10.3348/kjr.2017.18.1.113.
- [43] F. M. Candocia, “Simultaneous homographic and comparometric alignment of multiple exposure-adjusted pictures of the same scene,” *IEEE Trans. on Image Process.*, vol. 12, no. 12, pp. 1485–1494, Dec. 2003, doi: 10.1109/TIP.2003.819222.
- [44] T. Jinno and M. Okuda, “Multiple Exposure Fusion for High Dynamic Range Image Acquisition,” *IEEE Trans. on Image Process.*, vol. 21, no. 1, pp. 358–365, Jan. 2012, doi: 10.1109/TIP.2011.2160953.
- [45] S. Battiato, A. R. Bruna, and G. Puglisi, “A Robust Block-Based Image/Video Registration Approach for Mobile Imaging Devices,” *IEEE Transactions on Multimedia*, vol. 12, no. 7, pp. 622–635, Nov. 2010, doi: 10.1109/TMM.2010.2060474.
- [46] A. Zhu, H. Lu, and Z. Cao, “Video stabilization based on image registration,” *Journal of Electronic Imaging*, vol. 31, no. 2, pp. 023007–023007, 2022.